Topological Dissipative Photonics and Topological Insulator Lasers in Synthetic Time-Frequency Dimensions

Zhaohui Dong, Xianfeng Chen, Avik Dutt, and Luqi Yuan**

The study of dissipative systems has attracted great attention, as dissipation engineering has become an important candidate toward manipulating light in classical and quantum ways. Here, the behavior of a topological system is theoretically investigated with purely dissipative couplings in a synthetic time-frequency space. An imaginary bandstructure is shown, where eigen-modes experience different eigen-dissipation rates during the evolution of the system, resulting in mode competition between edge states and bulk modes. Numerical simulations show that distributions associated with edge states can dominate over bulk modes with stable amplification once the pump and saturation mechanisms are taken into consideration, which therefore points to a laser-like behavior for edge states robust against disorders. This work provides a scheme for manipulating multiple degrees of freedom of light by dissipation engineering, and also proposes a great candidate for topological lasers with dissipative photonics.

1. Introduction

Dissipation naturally exists in many physical systems and hence attracts broad interest. Through dissipation engineering, physical states of systems can be manipulated[1–4] in fields of ultra-cold atoms,[5–7] superconducting circuits,[8–10] and photonics.[11–13] On the other hand, topological photonics shows non-trivial one-way edge states robust against imperfections.[14–19] Therefore, combination of dissipation engineering and topology brings new physical phenomena and provides potential applications in controlling quantum or classical states, such as directional amplifiers,[12] quantum frequency locking,[20] and quantum computation.[21]

Recent research on dissipative physics explores systems with complex couplings in lattice models in the real space.[5,6,21,22] However, when the number of lattice sites or the dimension of the system increases, the problem associated with spatial complexity becomes inevitable. Synthetic dimensions,[23–25] however, provide alternative methods by utilizing other degrees of freedom of the system to reduce the spatial complexity. By connecting discrete modes, artificial lattices with desired complex couplings can be constructed in synthetic dimensions,[26–32] providing a convenient way for studying topological physics with large-scale Hamiltonians or in high-dimensional systems.[33–41] Moreover, synthetic dimensions bring exotic opportunities for manipulating different properties of light.[42–49] Recently, topological dissipation in a synthetic time dimension has been studied by creating a time-multiplexed resonator network.[50]

In this paper, we theoretically study a dissipative synthetic 2D time-frequency lattice model in a modulated resonator with multiple distinct circulating pulses. Dissipative couplings are introduced through auxiliary delay lines to connect pulses at different arrival times.[50] We propose to use amplitude modulator (AM) to induce complex-valued connectivities between discrete frequency modes of pulses to construct the synthetic frequency dimension. A synthetic 2D imaginary quantum Hall model is then built and its bandstructure exhibits topological dissipation with imaginary eigenvalues. We find that the field distribution initially localized at boundaries associated to edge states dominates initially but may eventually disappear because bulk bands hold larger negative imaginary eigenvalues (gain). However, by introducing saturation and external pump source, we obtain laser-like behavior for topological edge states, robust against disorders, which points toward topological lasers with synthetic dimensions.

Z. Dong, X. Chen, L. Yuan
State Key Laboratory of Advanced Optical Communication Systems and Networks, School of Physics and Astronomy
Shanghai Jiao Tong University
Shanghai 200240, China
E-mail: yuanluqi@sjtu.edu.cn

X. Chen
Shanghai Research Center for Quantum Sciences
Shanghai 201315, China

X. Chen
Collaborative Innovation Center of Light Manipulation and Applications
Shandong Normal University
Jinan 250358, China

A. Dutt
Department of Mechanical Engineering, and Institute for Physical Science and Technology
University of Maryland
College Park, MD 20742, USA
E-mail: avikdutt@umd.edu

A. Dutt
National Quantum Laboratory (QLab) at Maryland
College Park, MD 20742, USA

The ORCID identification number(s) for the author(s) of this article can be found under https://doi.org/10.1002/lpor.202300354

DOI: 10.1002/lpor.202300354

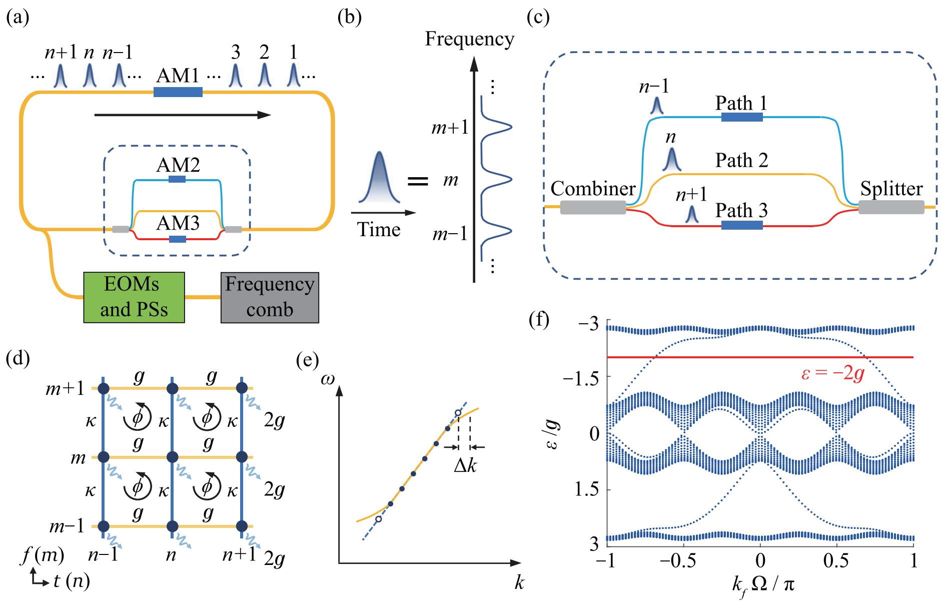

Figure 1. a) Scheme of the cavity loop. The initial pulse chain and the external pumps are prepared by modulating strengths and phases of all frequency components of each frequency comb signal in real time by electro-optic modulators (EOMs) and phase shifters (PSs). b) Each pulse may carry multiple frequency modes, separated by Ω. c) Zoom-in of part including delay lines. d) A dissipative lattice in 2D synthetic time-frequency space. e) Dispersion of waveguide that composes the cavity (yellow line). The dashed line represents a linear dispersion. Solid dots denote frequency modes, and hollow dots represent modes out of linear dispersion regime, introducing wavevector mismatch Δk. f) Projected bandstructure with $\kappa = g$ and $\phi = \pi/2$. Red line denotes $\varepsilon = -2g$.

2. Model

We study a chain of N pulses, separated with time interval T, circulating inside a cavity loop with the roundtrip time T_r in **Figure** 1a. To construct the synthetic frequency dimension, AM1 is placed in the main cavity, described by a modulation function $\Gamma = 1 - 2\alpha \cos[\Omega(t - z \cdot n_g/c)]$. Here $\alpha \ll 1$ is the modulation strength, Ω is the modulation frequency, c is the speed of light in vacuum, and n_g is the corresponding refractive index for the loop, which is considered to be the same for all frequency components in each pulse by assuming zero group velocity dispersion around the reference frequency ω_0. Such kind of frequency modulation[48,51,52] produces sidebands around the original frequency spaced by Ω, thereby connecting discrete frequency components at $\omega_m = \omega_0 + m\Omega$ and creating a synthetic lattice in frequency dimension, with m being an integer. Given N and T_r, each pulse has a temporal width $\ll T_r/N$ to prevent temporal overlaps. To ensure that all frequency components in each pulse are well separated in the frequency axis, we require the spectral width of each frequency component $\ll \Omega$, so each pulse holds a frequency-comb-like spectrum as shown in Figure 1b (see Supporting Information for detailed explanation of the balance between the spectral width of each frequency component and the temporal width of each pulse).

The cavity loop includes a pair of delay lines (see Figure 1c), which provides dissipative couplings in time dimension.[50] In detail, for the n-th pulse passing the splitter, a small portion of the pulse leaks into path 1 (3). The length of path 1 (3) is longer (shorter) than that of path 2 by $\Delta L = cT/n_g$. Therefore, the pulse that propagates through path 1 (3) is delayed (advanced) by T, i.e., encountering its nearby pulse at the combiner, which hence forms the synthetic lattice in time. Note that here, each pulse carries multiple frequency components separated by Ω as shown in Figure 1b, so compared with that passing path 2, each frequency component at ω_m passing path 1 or 3 accumulates an additional phase $\pm(\phi_0 + m\phi) = \pm k_m \Delta L = \pm(\omega_0 + m\Omega) n_g \Delta L/c$, where k_m is the wavevector, $\phi_0 \equiv \omega_0 n_g \Delta L/c$, and $\phi \equiv \Omega n_g \Delta L/c$.

This proposed system in Figure 1a supports a non-Hermitian model. The modulation of the active device AM1 varies the amplitude of the field sinusoidally, which brings imaginary coupling in the frequency dimension. Meanwhile, the couplings between different pulses are connected in an indirect way mediated by the delay lines. Such delay lines analogously play the role of external reservoirs, providing non-Hermitian connectivity between pulses in the time dimension.[50] Therefore, a 2D lattice can be built in the time-frequency synthetic space, described by Hamiltonian (see Supporting Information):

$$\tilde{H} = -\sum_{m,n} ig\left[b^\dagger_{m,n+1} b_{m,n} + b^\dagger_{m,n} b_{m,n+1}\right] - \sum_{m,n} i\kappa \left[e^{-in\phi} b^\dagger_{m+1,n} b_{m,n} + e^{in\phi} b^\dagger_{m,n} b_{m+1,n}\right] \tag{1}$$

where $b_{m,n}$ and $b^\dagger_{m,n}$ are annihilation and creation operators for the m-th frequency mode of the n-th pulse, g is the normalized coupling amplitude between nearby pulses, and $\kappa = \alpha/T_r$ is the normalized coupling amplitude along the frequency axis. Such system has an intrinsic global loss rate at $2g$ originating from the delay lines (see Supporting Information).

The anti-Hermitian Hamiltonian (1) gives 2D dissipative lattice structure in synthetic time-frequency space (see Figure 1d). We then consider building a finite lattice model in the synthetic time-frequency space (i.e., under open boundary conditions (OBCs)). To form an OBC in time dimension, we propose to

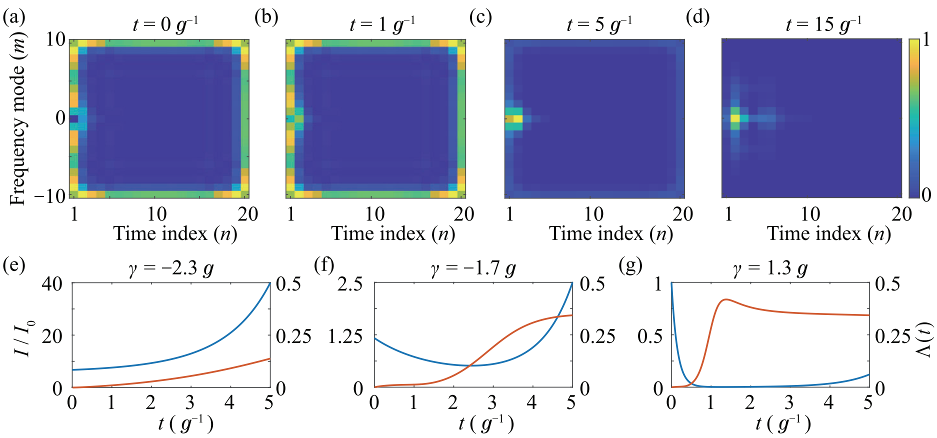

Figure 2. a) Normalized $|\nu_{m,n}|^2$ with $\gamma = -2.3$. Distributions of $|\nu_{m,n}|^2$ at different times, with b) $t = 1g^{-1}$, c) $t = 5g^{-1}$, and d) $t = 15g^{-1}$. Evolutions of I (blue lines) and $\Lambda(t)$ (red lines) for e) $\gamma = -2.3g$, f) $\gamma = -1.7g$, and g) $\gamma = 1.3g$, respectively.

place AM2 (AM3) in path 1 (3) acting like a dynamical switch. By carefully setting the switching-off time slot, we can cut off the corresponding undesired coupling from one pulse to the other one. For the frequency dimension, one can create artificial boundaries by choosing the dispersion of the waveguide that composes the cavity, as shown in Figure 1e, so only frequency modes hold resonant couplings are considered.[29]

We first plot projected bandstructure onto the wavevector that is reciprocal to the frequency dimension, if we consider 20 pulses with infinite frequency modes in Equation (1), with $\kappa = g$ and $\phi = \pi/2$. The corresponding projected bandstructure is plotted in Figure 1f, where ε is imaginary eigenvalue of the Hamiltonian and k_f is the quasimomentum reciprocal to the frequency axis.[52] $\tilde{H}$ possesses exclusively imaginary eigenvalues, suggesting each eigen-mode experiences different dissipation rate ε, instead of usual eigenvalues associated with eigen-frequencies in a Hermitian Hamiltonian. Here, a negative ε represents gain, while a positive one represents loss. Note that there is an intrinsic global loss of $2g$ in the system (see Supporting Information), so only eigenmodes with $\varepsilon < -2g$ may have gain. The global loss $2g$ is fixed unless a different method is used to connect different pulses in the time dimension. However, one may seek a larger range of ε for edge modes with gain by choosing other parameters (e.g., tuning κ/g, see Supporting Information). Moreover, one notes $\tilde{H} = iH_c$, where H_c is a conservative Hamiltonian supporting a non-zero effective magnetic flux in 2D synthetic space in the current case.[53] Therefore, topological invariants of bands in Figure 1f are identical to the ones for H_c, since the spectrum of $\tilde{H}$ is the same as H_c except for the additional i for the eigenvalues, indicating that our system supports topological edge states, but in a dissipative way. We briefly discuss on the topological invariant of the system in the Supporting Information.

We further study a finite lattice by considering 20 pulses ($n \in [1, 20]$) circulating inside the loop, each of which includes 21 resonant modes ($m \in [-10, 10]$). The evolution equation is,

$$\frac{d|\Psi\rangle}{dt} = -(i\tilde{H} + 2g)|\Psi\rangle + S \tag{2}$$

here, $|\Psi\rangle = \sum_{m,n} \nu_{m,n}(t) b^{\dagger}_{m,n}|0\rangle$, where $\nu_{m,n}(t)$ is the field amplitude at the m-th mode in the n-th pulse, and S denotes external pump source. If we assume $\nu_{m,n}(t) = \tilde{\nu}_{m,n} e^{-(\gamma+2g)t}$, where γ represents the expected dissipation rate, and consider only the site (0,1), i.e., the 0-th mode at the 1-st pulse, is externally pumped at the strength p, we obtain,[54]

$$g\left(\tilde{\nu}_{m,n+1} + \tilde{\nu}_{m,n-1}\right) + \kappa\left(e^{-in\phi}\tilde{\nu}_{m-1,n} + e^{in\phi}\tilde{\nu}_{m+1,n}\right) - \gamma\tilde{\nu}_{m,n} = p\delta_{m,0}\delta_{n,1} \tag{3}$$

We set $p = \kappa = g$, choose $\gamma = -2.3g$ to excite edge states in Figure 1f, and diagonalize Equation (3) to obtain the initial distribution of $\nu_{m,n}(0) = \tilde{\nu}_{m,n}$ as shown in **Figure 2**a. Such choice of γ results in the energy of the system distributed at boundaries of the synthetic space. We next numerically simulate the evolution of the system when one initially prepares the system following different distributions of $\tilde{\nu}_{m,n}$ and study the mode competitions from the dissipative lattice model. Now we apply the initial distribution $\tilde{\nu}_{m,n}$, which can be prepared by injecting all pulses with desired frequency distributions following $\tilde{\nu}_{m,n}$, and solve Equation (2) without external pump. Distributions of normalized $|\nu_{m,n}|^2$ at different t are plotted in Figure 2b–d. Intensity distributions gradually leak into the bulk sites (a clearer bulk feature is provided with longer t, see Supporting Information), which fundamentally differs from the case of a corresponding conservative system. The reason is that not only the desired edge states at $\varepsilon = -2.3g$, but also a small portion of other states including bulk modes with larger negative dissipation rates $|\varepsilon| \approx 2.7g$ are initially excited. Although the energy localized in edge states is dominant initially, it gradually transfers to bulk states that have larger negative ε, as a result of mode competitions (see Supporting Information for details). In experiments, γ can be tuned by amplifier inside the main loop. We also perform simulations with initial distributions of $\nu_{m,n}$ using $\gamma = -1.7g$ and $\gamma = 1.3g$, respectively, linked to edge states, and similar phenomena are observed (see Supporting Information). However, evolutions of total intensity $I \equiv \sum_{m,n} |\nu_{m,n}|^2$ are different (see Figure 2e–g). Here I_0 denotes reference intensity associated to initial distribution in Figure 2a. For the case with $\gamma < -2g$, I monotonously increases, while for cases with $\gamma > -2g$, I first decreases and later increases then when modes with larger negative ε dominate eventually as a result of mode competitions (see

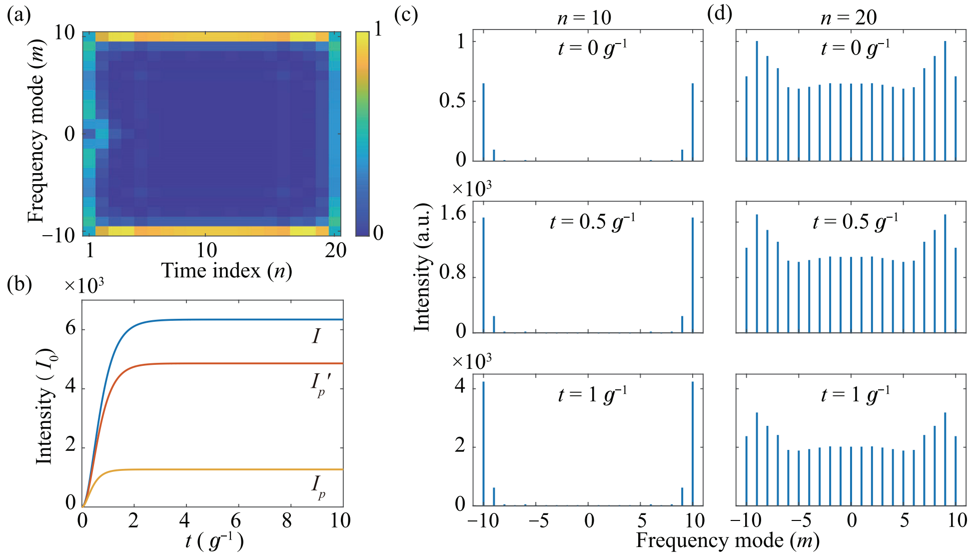

Figure 3. a) Intensity distribution of the steady state for simulating topological laser with Equation (4). b) Evolutions of I, $I_p{}'$, and I_p. Intensity distributions for c) 10-th pulse, and d) 20-th pulse at $t = 0g^{-1}$, $t = 0.5g^{-1}$ and $t = 1g^{-1}$.

the Supporting Information for a simple example in explaining the underlying physics). Moreover, we also define a coefficient $\Lambda(t) \equiv \sqrt{\sum_{m,n}(|v_{m,n}|^2/\sum_{m',n'}|v_{m',n'}|^2 - |\tilde{v}_{m,n}|^2/\sum_{m',n'}|\tilde{v}_{m',n'}|^2)^2}$ to describe the similarity of intensity distributions of the system at different evolution times t and the initial distribution $\tilde{v}_{m,n}$. $\Lambda(t) = 0$ when the intensity distributions of $v_{m,n}$ and $\tilde{v}_{m,n}$ are exactly the same, and $\Lambda(t)$ reaches its maximum $\sqrt{2}$ if $v_{m,n}$ and $\tilde{v}_{m,n}$ are completely not overlapped for all sites. We plot $\Lambda(t)$ with $\gamma = -2.3g$, $\gamma = -1.7g$ and $\gamma = 1.3g$ as the red lines in Figures 2e–g. For $\gamma = -2.3g$, $\Lambda(t)$ stays at a small value (< 0.02) before $t = 1.6g^{-1}$ and gradually increases at longer t, indicating qualitatively that the edge states initially dominate but as the system evolves, the energy distribution is no longer the desired edge state. For $\gamma = -1.7g$ and $\gamma = 1.3g$, $\Lambda(t)$ stays small when $t < 1.4g^{-1}$ and $t < 0.5g^{-1}$, respectively. After that, $\Lambda(t)$ experiences a large increase. One can find that such critical time is also the time when I turns from decreasing to increasing as the bulk states having larger negative ϵ become dominating.

3. Result

Although the dissipative topology here only exhibits features of topologically-protected edge states at small time that are eventually dominated by bulk modes with larger gains at longer time, the system still holds the capability for the realization of a topological laser. To this purpose, we add a saturation term into Equation (2) and evolutions of $v_{m,n}$ are:

$$\dot{v}_{m,n} = -g\left(v_{m,n+1} + v_{m,n-1}\right) - \kappa\left(e^{-in\phi}v_{m-1,n} + e^{in\phi}v_{m+1,n}\right) - 2gv_{m,n} + p_{m,n} - \frac{|\gamma|\sum_m |v_{m,n}|^2}{2gI_s/(-\gamma-2g) + \sum_m |v_{m,n}|^2}\cdot v_{m,n} \tag{4}$$

The last term in Equation (4) describes the saturation mechanism for the n-th pulse, which is dependent on the total intensity of all frequency components in each pulse, with saturation intensity set as $I_s = 25.7I_0$.[55] $\gamma = -2.3$ to satisfy $-\gamma - 2g > 0$. We pump the system via $p_{m,n}$, which obeys the distribution in Figure 2a, i.e., we inject pulse sequences following $p_{m,n}$ into the system at every roundtrip. To achieve this, frequency combs can be used, with amplitudes and phases at each ω_m following $p_{m,n}$, and are injected into the loop at the n-th time slot (see Figure 1a). The system reaches a steady-state distribution shown in **Figure 3**a, which exhibits non-symmetric feature and is different from the eigenstate distribution in Figure 2a. The reason is that the saturation term for $v_{m,n}$ depends on summation of intensities on all frequency modes in the n-th pulse but edge states exhibit different distributions on frequency modes for the 1-st, 20-th pulses and the rest pulses. Therefore, one can see larger intensity distribution on the ± 10-th modes in pulses with $n \in [2, 19]$ while nearly equal distributions on all modes in the 1-st and 20-th pulses. Figures 3c and 3d show intensity distributions in the 10-th and 20-th pulses at different times. To show the laser-like behavior, we also plot evolutions of total intensity $I = \sum_{m,n}|v_{m,n}|^2$ in Figure 3b. We compare I with the pump intensity I_p injected into the loop, which is calculated by solving Equation (4) with $\kappa = g = 0$, i.e., no coupling terms in synthetic time-frequency dimensions. Furthermore, if we further ignore the loss term $-2gv_{m,n}$ and then solve Equation (4) with $\kappa = g = 0$, we obtain the pure pump intensity $I_p{}'$. One sees that I increases faster than both I_p and $I_p{}'$ initially and becomes saturated at $t \approx 2.4g^{-1}$. We emphasize that the gain for the edge state mainly originates from the imaginary eigenvalue of the edge state supported by the system rather than the external pump (from the comparison between I and I_p). The effect of the pump is to temporarily provide extra gain for edge states, keeping them dominant over bulk modes before saturation. Figure 3 implies that such topological dissipative photonics in the time-frequency space can be applied to a topological laser in synthetic dimensions.[55]

Different from the topological laser that pumps the gain medium in a conservative topological system,[55–57] we directly

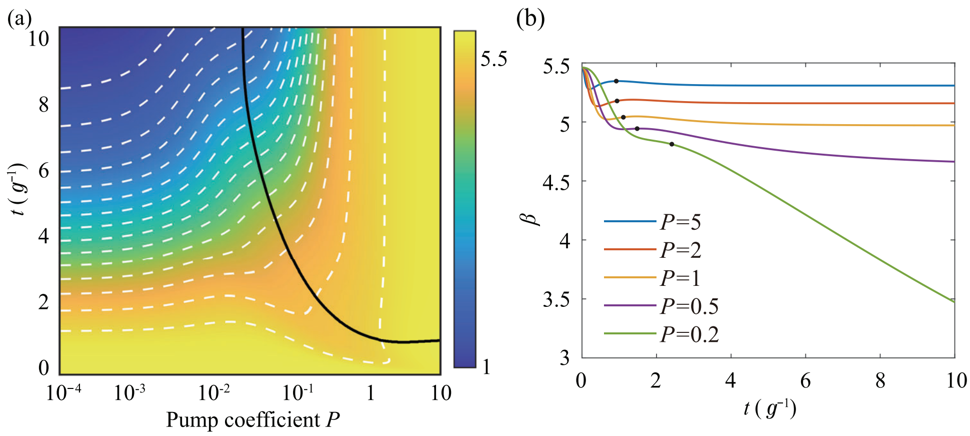

Figure 4. a) β versus time and P. White dashed lines denote equi-β lines. The black solid line represents the saturation time. b) β versus time for different P. black dots represent the saturation time, respectively.

start with an exclusively dissipatively coupled system where the eigenstate with purely imaginary eigenvalue intrinsically has gain/loss. For a topological laser,[55–57] gain originates from the external pump source since the system only supports real eigenvalues if the external pump is excluded. The on-site gain provided by the external pump has no relevance to the eigenvalue of each mode. While in our model, gain/loss comes from the imaginary eigenvalues and thus edge modes and bulk modes have different gain/loss coefficients. Therefore, the implementation of the topological laser from the dissipative photonics is not straightforwad, as bulk modes may have larger gains. We also compare effects of two simpler pump profiles (see Supporting Information), which shows that the response of the system is affected by the pump profile, so the current choice of a complex pump profile leads to better gain performance. This complex pump profile can be somehow simplified by only keeping most of the profile at boundaries in the synthetic space, which could be easier for the purpose of experiments (see Supporting Information).

We further investigate intensity distribution by varying the pump energy. In detail, we replace the pump term in Equation (4) by $P \cdot p_{m,n}$, where P gives the pump coefficient that linearly changes amplitudes of pump pulses, so for $P = 1$, the pump is the one used in Figure 3. We study distributions of edge and bulk modes during evolutions with different P in **Figure** 4a, by defining the edge-bulk ratio $\beta = I_e/I_b$, where $I_e \equiv \sum_{(m,n)} |v_{m,n}|^2$ with (m, n) referring to all sites at boundaries in the synthetic space and $I_b \equiv I - I_e$. One can see that for small P, the system initially holds a larger β, where most of the energy is localized at modes around boundaries. However, with the time evolution, β decreases and the bulk modes are excited. On the other hand, for large P, large β exists for a long time, indicating the persistence of edge modes during evolution. The saturation time, defined as the time when the increasing slope of the total intensity drops to half of its maximum, (see black line in Figure 4a) and characterizing the time that the system reaches saturation, decreases when P is increasing. To further understand such properties, we can classify P into two regimes, i.e., $P \leqslant 0.01$ for the weak pump regime and $P > 0.1$ for the strong pump regime. For the strong pump regime, the system gets saturated within the time $t \leqslant 10g^{-1}$. However, β may still drop for smaller P. In Figure 4b, we plot β versus t for several choices of P. One sees that β keeps at high ratio (> 4.5) for $P \geqslant 0.5$, but decreases for the case of $P = 0.2$ (see the Supporting Information for details). In particular, for $P > 0.5$ the edge-state-like distribution can be maintained for a very long time, and the corresponding saturation time $\approx 1g^{-1}$. For example, when $P = 1$, we can see that β has a value > 4.8 for $t > 10g^{-1}$ as shown in Figure 4b. Nevertheless, for a small $P = 0.01$, the edge-state-like distribution can only exist (with $\beta > 4.8$) before $t = 2g^{-1}$.

The features in the proposed synthetic time-frequency space exhibit dissipation but still hold topological properties. To demonstrate the topological protection, we introduce disorders in couplings terms. Specifically, the disorder of the couplings along the frequency axis may originate from the fluctuation of the modulation strength α in AM1. For all couplings between different frequency components, the disorder acts identically, and the coupling amplitude κ in for the n-th pulse in Equation (4) becomes $\kappa \rightarrow \kappa(1 + \delta \cdot R_n)$, where δ denotes the disorder strength, and R_n is a random number taken from $[-0.5, 0.5]$. On the other hand, the coupling between the main cavity and delay lines can also brings disorders. We take the coupling from the n-th pulse to the $(n \pm 1)$-th pulse as $g \rightarrow g(1 + \delta \cdot R_{\pm,n})$, regardless of the frequency index m, where $R_{\pm,n}$ are also random numbers taken from $[-0.5, 0.5]$. We perform simulations same as those in Figures 3a,b but including disorders with $\delta = 0.1$ and 0.5, respectively (see results in **Figure 5**). We find that both steady-state distributions and intensity evolutions exhibit similar characteristics as those in Figures 3a,b, showing that the effect of disorder is negligible, and the proposed system, though dissipative, still exhibits topological protection. To further demonstrate the properties of topological lasing, we plot output total intensity $\bar{I}$ versus the stable pure pump intensity $\bar{I}_p{}'$ with $\delta = 0$ (no disorder), $\delta = 0.1$ and $\delta = 0.5$ in Figure 5d–f, where $\bar{I}$ ($\bar{I}_p{}'$) is taken as the saturation value of I ($I_p{}'$), such as that shown in Figure 3b for $P = 1$. One finds that the threshold pump intensity in Figure 5d is about $1.5 \times 10^3 I_0$, which corresponds to a pump coefficient $P = 0.3$. Above the threshold, $\bar{I}$ grows linearly with $\bar{I}_p{}'$. In addition, the results in Figure 5e,f show similar features as Figure 5d, which indicates the robustness of the topological lasing against disorders.

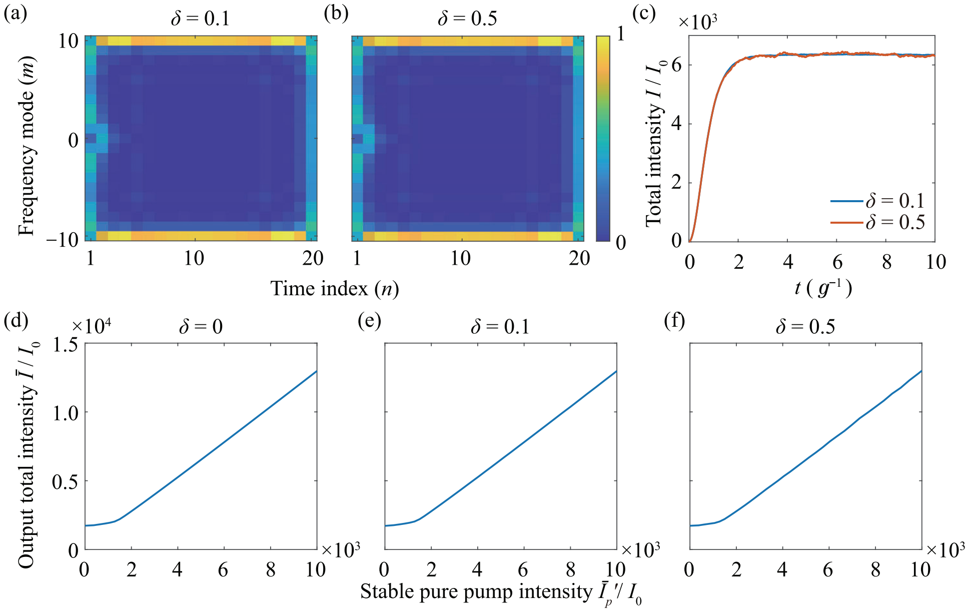

Figure 5. Intensity distribution of the steady state with disorders included, where a) $\delta = 0.1$ b) and $\delta = 0.5$. c) Evolutions of I versus time. d–f) The output total intensity $\bar{I}$ as a function of the stable pure pump intensity $\bar{I}_p'$ with d) $\delta = 0$, e) $\delta = 0.1$, and f) $\delta = 0.5$.

Next, we present the study of the size effects on the proposed system in simulations. We compare the steady state distributions and evolutions of the total intensity I for models with the lattice size as 11×10, 21×20, and 41×40, respectively, which are shown in **Figure 6**. The saturation intensity is set as $I_s = 25.7 I_0$, where I_0 varies for the cases of different lattice sizes. The initial states and the pump profiles are obtained following the way in the previous section with $\gamma = -2.3g$ and pump coefficient $P = 1$. One can find that for a smaller lattice size, more energy penetrates into the bulk sites, indicating that the topological protection is weaker. Moreover, the intensity distribution for $n = 1$ is larger than the one for $n = 10$ due to the intensity distribution of the initial state and the pump profile we select. However, one can see that if the larger lattice size is chosen, the total intensity I becomes larger. Moreover, as it can be seen in Figure 6c, the distribution of the edge state becomes much more clearer, which shows that a system with larger size has better topological protection for edge states. In particular, for pulses with $n \in [2, 39]$, one can clearly see the amplification of modes at edge, i.e., $m = 20$ and $m = -20$. Such results may have an advantage in utilizing the lasing property of the edge state in the time-frequency space in a more efficient way.

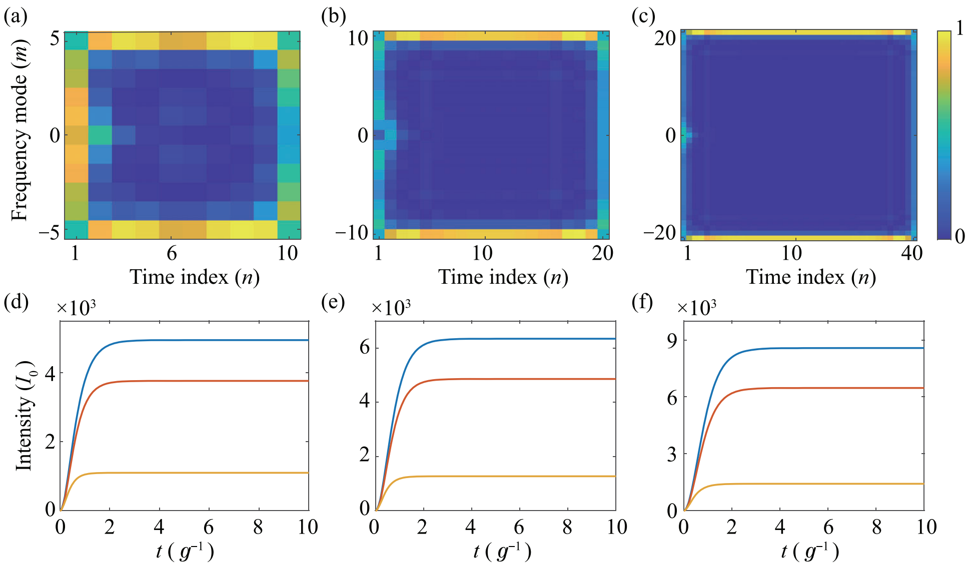

Figure 6. Intensity distributions of the steady state for models with the lattice size as a) 11×10, b) 21×20, and c) 41×40 lattice size, respectively. d–f) Corresponding evolutions of I (blue line), I_p' (red line), and I_p (yellow line) versus time.

4. Discussion

Our proposal is experimentally feasible in a fiber network.[50] We emphasize that the separation of modes in both time and frequency dimensions should be larger than their corresponding full width at half maximum (FWHM).[48] This requires that FWHM in time for each pulse is smaller than T and FWHM in frequency for each mode is smaller than Ω. For example, for a loop supporting $T_r \approx 200$ ns, if there are $N = 20$ pulses circulating, each pulse can have a temporal width $\approx$ 1 ns to ensure that the pulses are separated in time. This then requires a modulation ≈ 10 GHz in frequency so that each pulse supports discretely spaced spectral components with the spectral width $\approx$1 GHz[58] (see Supporting Information for details). Furthermore, recent developments of on-chip integrated photonic technologies could also provide another possible experimental platform.[59,60] Limitations of our proposal may come from the additional losses from the propagation inside the loop, connections between components, etc. and also the challenge in synchronizing signal and pump pulses.

The major difference between our work and Ref. [50] is the strategy of realizing the dissipatively coupled system (i.e., the inclusion of synthetic frequency dimension). AM1 in the main cavity not only simply connects the sites in the frequency dimension, but also plays a crucial role as exchanging energy between the system and the external reservoir, which distinguishes our work from previous works.[21,50,61] Besides, the dissipative couplings in frequency dimension from AM also differentiate our model from non-Hermitian models based on either on-site gain/loss[62] or direction-dependent gain/loss coupling.[63] Although the proposed dissipative topological photonics may also be implemented using pulses in the time-multiplexed network,[50] our proposal in synthetic time-frequency dimensions carries several possible advantages, summarized in the following. First, the proposed scheme supports the eigenstate with purely imaginary eigenvalue intrinsically having gain, whereby amplitude modulations provide extra energy. Second, the effective magnetic flux comes in automatically without requiring additional delay lines and more modulators that may cause more insertion loss. In addition, the achievement of a $N \times N$ lattice model in synthetic time-frequency dimensions avoids the quadratic increase in the required number of pulses N and hence the length of the loop, which therefore reduces the spatial footprint and complexity. Lastly, by modulating pulses with the additional frequencies at multiples of Ω, our study can be flexibly generalized to models with long-range couplings[49,64] or extended to higher dimensions,[37,65–67] without adding additional delay lines or increasing the size of the optical loop. Our work therefore offers new opportunities in manipulating multiple properties of light and points toward topological lasers with synthetic dimensions.[55–57,68–70]

In summary, we propose a way to generate artificial lattices in a 2D synthetic time-frequency space and explore physical phenomena associated with dissipative photonics. The system supports imaginary eigenvalues, which results in gain for edge states. We study mode competition phenomena between edge states and bulk bands. By introducing saturation, we explore laser-like amplification with the topological protection, and find a way to excite such a lasing edge mode and preserve its dominance with the topological protection. From an application point of view, the proposed synthetic topological amplification naturally supports spectrotemporally shaped lasing emission as it is achieved by a pulse chain carrying multiple frequency components. In addition, such synchronous amplification of multiple temporal pulses including many frequency components is robust against disorder, which may be technically challenging.[55,71] The proposed system with further designs can provide a realistic approach for further performing quantum simulations such as mimicking the quantum spin-Hall phase,[72–74] and also studying non-Hermitian physics and understanding dissipative topological systems.[63,75–78]

Supporting Information

Supporting Information is available from the Wiley Online Library or from the author.

Acknowledgements

The research was supported by the National Natural Science Foundation of China (12122407, 11974245, and 12192252), National Key Research and Development Program of China (no. 2021YFA1400900 and no. 2023YFA1407200). L.Y. thanks the sponsorship from Yangyang Development Fund and the support from the Program for Professor of Special Appointment (Eastern Scholar) at Shanghai Institutions of Higher Learning. A.D. acknowledged support through the University of Maryland startup grant, and through grants from Northrop Grumman University Research Program and the National Quantum Lab (Q-Lab by UMD and IonQ).

Conflict of Interest

The authors declare no conflict of interest.

Data Availability Statement

The data that support the findings of this study are available from the corresponding author upon reasonable request.

Keywords

dissipative photonics, synthetic dimensions, topological laser, topological photonics

Received: April 23, 2023
Revised: July 30, 2023
Published online:

[1] M. B. Plenio, S. F. Huelga, A. Beige, P. L. Knight, *Phys. Rev. A* **1999**, *59*, 2468.
[2] F. Verstraete, M. M. Wolf, J. Ignacio Cirac, *Nat. Phys.* **2009**, *5*, 633.
[3] B.-H. Liu, L. Li, Y.-F. Huang, C.-F. Li, G.-C. Guo, E.-M. Laine, H.-P. Breuer, J. Piilo, *Nat. Phys.* **2011**, *7*, 931.
[4] S. Zippilli, D. Vitali, *Phys. Rev. Lett.* **2021**, *126*, 020402.
[5] S. Diehl, A. Micheli, A. Kantian, B. Kraus, H. Büchler, P. Zoller, *Nat. Phys.* **2008**, *4*, 878.
[6] S. Diehl, W. Yi, A. Daley, P. Zoller, *Phys. Rev. Lett.* **2010**, *105*, 227001.

[7] K. Seetharam, A. Lerose, R. Fazio, J. Marino, *Phys. Rev. Res.* **2022**, *4*, 013089.
[8] M. Mirrahimi, Z. Leghtas, V. V. Albert, S. Touzard, R. J. Schoelkopf, L. Jiang, M. H. Devoret, *New J. Phys.* **2014**, *16*, 045014.
[9] J. Cohen, M. Mirrahimi, *Phys. Rev. A* **2014**, *90*, 062344.
[10] I. Siddiqi, *Nat. Rev. Mater.* **2021**, *6*, 875.
[11] T. J. Kippenberg, A. L. Gaeta, M. Lipson, M. L. Gorodetsky, *Science* **2018**, *361*, eaan8083.
[12] C. C. Wanjura, M. Brunelli, A. Nunnenkamp, *Nat. Commun.* **2020**, *11*, 3149.
[13] L. G. Wright, P. Sidorenko, H. Pourbeyram, Z. M. Ziegler, A. Isichenko, B. A. Malomed, C. R. Menyuk, D. N. Christodoulides, F. W. Wise, *Nat. Phys.* **2020**, *16*, 565.
[14] Y. Hatsugai, *Phys. Rev. Lett.* **1993**, *71*, 3697.
[15] Z. Wang, Y. Chong, J. D. Joannopoulos, M. Soljačić, *Nature* **2009**, *461*, 772.
[16] M. Z. Hasan, C. L. Kane, *Rev. Mod. Phys.* **2010**, *82*, 3045.
[17] X.-L. Qi, S.-C. Zhang, *Rev. Mod. Phys.* **2011**, *83*, 1057.
[18] T. Ozawa, H. M. Price, A. Amo, N. Goldman, M. Hafezi, L. Lu, M. C. Rechtsman, D. Schuster, J. Simon, O. Zilberberg, I. Carusotto, *Rev. Mod. Phys.* **2019**, *91*, 015006.
[19] H. Price, Y. Chong, A. Khanikaev, H. Schomerus, L. J. Maczewsky, M. Kremer, M. Heinrich, A. Szameit, O. Zilberberg, Y. Yang, B. Zhang, A. Alù, R. Thomale, I. Carusotto, P. St-Jean, A. Amo, A. Dutt, L. Yuan, S. Fan, X. Yin, C. Peng, T. Ozawa, A. Blanco-Redondo, *J. Phys.: Photonics* **2022**, *4*, 032501.
[20] F. Nathan, G. Refael, M. S. Rudner, I. Martin, *Phys. Rev. Res.* **2020**, *2*, 043411.
[21] K. Fujii, M. Negoro, N. Imoto, M. Kitagawa, *Phys. Rev. X* **2014**, *4*, 041039.
[22] A. Metelmann, A. A. Clerk, *Phys. Rev. X* **2015**, *5*, 021025.
[23] A. Celi, P. Massignan, J. Ruseckas, N. Goldman, I. B. Spielman, G. Juzeliūnas, M. Lewenstein, *Phys. Rev. Lett.* **2014**, *112*, 043001.
[24] L. Yuan, Q. Lin, M. Xiao, S. Fan, *Optica* **2018**, *5*, 1396.
[25] E. Lustig, M. Segev, *Adv. Opt. Photonics* **2021**, *13*, 426.
[26] O. Boada, A. Celi, J. Latorre, M. Lewenstein, *Phys. Rev. Lett.* **2012**, *108*, 133001.
[27] A. Regensburger, C. Bersch, M.-A. Miri, G. Onishchukov, D. N. Christodoulides, U. Peschel, *Nature* **2012**, *488*, 167.
[28] X.-W. Luo, X. Zhou, C.-F. Li, J.-S. Xu, G.-C. Guo, Z.-W. Zhou, *Nat. Commun.* **2015**, *6*, 8949.
[29] L. Yuan, Y. Shi, S. Fan, *Opt. Lett.* **2016**, *41*, 741.
[30] T. Ozawa, H. M. Price, N. Goldman, O. Zilberberg, I. Carusotto, *Phys. Rev. A* **2016**, *93*, 043827.
[31] E. Lustig, S. Weimann, Y. Plotnik, Y. Lumer, M. A. Bandres, A. Szameit, M. Segev, *Nature* **2019**, *567*, 356.
[32] Y. Hu, C. Reimer, A. Shams-Ansari, M. Zhang, M. Loncar, *Optica* **2020**, *7*, 1189.
[33] S.-C. Zhang, J. Hu, *Science* **2001**, *294*, 823.
[34] H. M. Price, O. Zilberberg, T. Ozawa, I. Carusotto, N. Goldman, *Phys. Rev. Lett.* **2015**, *115*, 195303.
[35] B. Lian, S.-C. Zhang, *Phys. Rev. B* **2016**, *94*, 041105.
[36] M. Lohse, C. Schweizer, H. M. Price, O. Zilberberg, I. Bloch, *Nature* **2018**, *553*, 55.
[37] L. Yuan, M. Xiao, Q. Lin, S. Fan, *Phys. Rev. B* **2018**, *97*, 104105.
[38] D. Yu, B. Peng, X. Chen, X.-J. Liu, L. Yuan, *Light: Sci. Appl.* **2021**, *10*, 209.
[39] K. Wang, A. Dutt, K. Y. Yang, C. C. Wojcik, J. Vučković, S. Fan, *Science* **2021**, *371*, 1240.
[40] K. Wang, A. Dutt, C. C. Wojcik, S. Fan, *Nature* **2021**, *598*, 59.
[41] G. Li, L. Wang, R. Ye, Y. Zheng, D.-W. Wang, X.-J. Liu, A. Dutt, L. Yuan, X. Chen, *Light: Sci. Appl.* **2023**, *12*, 81.
[42] S.-L. Zhang, Q. Zhou, *J. Phys. B: At., Mol. Opt. Phys.* **2017**, *50*, 222001.
[43] X.-F. Zhou, X.-W. Luo, S. Wang, G.-C. Guo, X. Zhou, H. Pu, Z.-W. Zhou, *Phys. Rev. Lett.* **2017**, *118*, 083603.
[44] B. A. Bell, K. Wang, A. S. Solntsev, D. N. Neshev, A. A. Sukhorukov, B. J. Eggleton, *Optica* **2017**, *4*, 1433.
[45] C. Qin, F. Zhou, Y. Peng, D. Sounas, X. Zhu, B. Wang, J. Dong, X. Zhang, A. Alù, P. Lu, *Phys. Rev. Lett.* **2018**, *120*, 133901.
[46] A. Dutt, Q. Lin, L. Yuan, M. Minkov, M. Xiao, S. Fan, *Science* **2020**, *367*, 59.
[47] S. Weidemann, M. Kremer, T. Helbig, T. Hofmann, A. Stegmaier, M. Greiter, R. Thomale, A. Szameit, *Science* **2020**, *368*, 311.
[48] G. Li, D. Yu, L. Yuan, X. Chen, *Laser Photonics Rev.* **2022**, *16*, 2100340.
[49] G. Li, L. Wang, R. Ye, S. Liu, Y. Zheng, L. Yuan, X. Chen, *Adv. Photonics* **2022**, *4*, 036002.
[50] C. Leefmans, A. Dutt, J. Williams, L. Yuan, M. Parto, F. Nori, S. Fan, A. Marandi, *Nat. Phys.* **2022**, *18*, 442.
[51] Y. Song, W. Liu, L. Zheng, Y. Zhang, B. Wang, P. Lu, *Phys. Rev. Appl.* **2020**, *14*, 064076.
[52] L. Yuan, A. Dutt, S. Fan, *APL Photonics* **2021**, *6*, 071102.
[53] K. Fang, Z. Yu, S. Fan, *Nat. Photonics* **2012**, *6*, 782.
[54] T. Ozawa, I. Carusotto, *Phys. Rev. Lett.* **2014**, *112*, 133902.
[55] Z. Yang, E. Lustig, G. Harari, Y. Plotnik, Y. Lumer, M. A. Bandres, M. Segev, *Phys. Rev. X* **2020**, *10*, 011059.
[56] G. Harari, M. A. Bandres, Y. Lumer, M. C. Rechtsman, Y. D. Chong, M. Khajavikhan, D. N. Christodoulides, M. Segev, *Science* **2018**, *359*, eaar4003.
[57] M. A. Bandres, S. Wittek, G. Harari, M. Parto, J. Ren, M. Segev, D. N. Christodoulides, M. Khajavikhan, *Science* **2018**, *359*, eaar4005.
[58] A. Rueda, F. Sedlmeir, M. Kumari, G. Leuchs, H. G. Schwefel, *Nature* **2019**, *568*, 378.
[59] C. Wang, C. Langrock, A. Marandi, M. Jankowski, M. Zhang, B. Desiatov, M. M. Fejer, M. Lončar, *Optica* **2018**, *5*, 1438.
[60] A. Balčytis, T. Ozawa, Y. Ota, S. Iwamoto, J. Maeda, T. Baba, *Sci. Adv.* **2022**, *8*, eabk0468.
[61] M. Parto, C. Leefmans, J. Williams, F. Nori, A. Marandi, *Nat. Commun.* **2023**, *14*, 1440.
[62] S. Weimann, M. Kremer, Y. Plotnik, Y. Lumer, S. Nolte, K. G. Makris, M. Segev, M. C. Rechtsman, A. Szameit, *Nat. Mater.* **2017**, *16*, 433.
[63] K. Yokomizo, S. Murakami, *Phys. Rev. Lett.* **2019**, *123*, 066404.
[64] A. Dutt, M. Minkov, Q. Lin, L. Yuan, D. A. Miller, S. Fan, *Nat. Commun.* **2019**, *10*, 3122.
[65] A. Senanian, L. G. Wright, P. F. Wade, H. K. Doyle, P. L. McMahon, *Nat. Phys.* **2023**, *19*, 1333.
[66] D. Cheng, E. Lustig, K. Wang, S. Fan, *Light: Sci. Appl.* **2023**, *12*, 158.
[67] R. Ye, Y. He, G. Li, L. Wang, X. Wu, X. Qiao, Y. Zheng, L. Jin, D.-W. Wang, L. Yuan, et al., (Preprint) arXiv:2305.17853v1, **2023**.
[68] P. St-Jean, V. Goblot, E. Galopin, A. Lemaître, T. Ozawa, L. Le Gratiet, I. Sagnes, J. Bloch, A. Amo, *Nat. Photonics* **2017**, *11*, 651.
[69] M. Parto, S. Wittek, H. Hodaei, G. Harari, M. A. Bandres, J. Ren, M. C. Rechtsman, M. Segev, D. N. Christodoulides, M. Khajavikhan, *Phys. Rev. Lett.* **2018**, *120*, 113901.
[70] H. Zhao, P. Miao, M. H. Teimourpour, S. Malzard, R. El-Ganainy, H. Schomerus, L. Feng, *Nat. Commun.* **2018**, *9*, 981.
[71] Z. Chen, M. Segev, *ELight* **2021**, *1*, 2.
[72] C. L. Kane, E. J. Mele, *Phys. Rev. Lett.* **2005**, *95*, 226801.
[73] D. Sheng, Z. Weng, L. Sheng, F. Haldane, *Phys. Rev. Lett.* **2006**, *97*, 036808.
[74] B. A. Bernevig, S.-C. Zhang, *Phys. Rev. Lett.* **2006**, *96*, 106802.
[75] H. Shen, B. Zhen, L. Fu, *Phys. Rev. Lett.* **2018**, *120*, 146402.
[76] F. Song, S. Yao, Z. Wang, *Phys. Rev. Lett.* **2019**, *123*, 246801.
[77] S. Longhi, *Phys. Rev. Res.* **2019**, *1*, 023013.
[78] Y. Ashida, Z. Gong, M. Ueda, *Adv. Phys.* **2020**, *69*, 249.